Morphological Changes of Poly(ethylene terephthalate-*co*-isophthalate) During Solid State Polymerization

Stamatina N. Vouyiouka,[1] Viviane Filgueiras,[2] Constantine D. Papaspyrides,[1] Enrique L. Lima,[2] Jose Carlos Pinto[2]

[1]*Laboratory of Polymer Technology, School of Chemical Engineering, National Technical University of Athens, Zographou, Athens 15780, Greece*
[2]*Programa de Engenharia Química/COPPE, Universidade Federal do Rio de Janeiro, Cidade Universitária-CP: 68502, 21941-972 Rio de Janeiro, RJ, Brazil*

Received 24 February 2011; accepted 9 August 2011
DOI 10.1002/app.35452
Published online 2 December 2011 in Wiley Online Library (wileyonlinelibrary.com).

ABSTRACT: Poly(ethylene terephthalate-*co*-isophthalate) (PETI) prepolymer was submitted to solid state polymerization (SSP) at 184–230°C in a fixed bed reactor, to study the evolution of morphological changes during the process. Short reaction times were selected to investigate crystallization phenomena during nonisothermal (heating) and isothermal SSP phases. More specifically, multiple PETI melting behavior was observed and attributed to secondary crystallization, the rate of which increased significantly with SSP temperature. Reaction time was also found to exert a positive effect on solid-phase perfection of secondary crystals, leading at each temperature to melting points close to the value of bottle-grade poly(ethylene terephthalate). Finally, the mass fraction crystallinity of the SSP grades was found to comply with the crystal morphology encountered.
 J Appl Polym Sci 124: 4457–4465, 2012

Key words: solid state polymerization; poly(ethylene terephthalate); cold crystallization; crystallinity degree; secondary crystallization

INTRODUCTION

Poly(ethylene terephthalate) (PET) is an important polymer, corresponding to 7% of plastics demand in Europe.[1] PET is used commercially for production of bottles as a copolymer grade of ethylene terephthalate and ethylene isophthalate [poly(ethylene terephthalate-*co*-isophthalate) (PETI)] and constitutes an important family of commodity plastics, especially for packaging applications, with a market value of 1.36–1.50 \$ kg^{-1}.[2] In particular, PET is widely used in fibers, films, and container applications, including the fabrication of bottles for beverages, soft drinks, fruit juices, mineral waters, carbonated drinks, etc. PET is also used for production of trays with precooked meals and tire cords. Depending on the final application, different intrinsic viscosities (IVs) are required for PET grades, as presented in Table I.[3]

To produce PET with IV of 0.6 dL g^{-1}, melt polymerization processes are normally employed, involving the bulk reaction of ethylene glycol with dimethyl terephthalate or purified terephthalic acid. The reaction mass flows through a series of reactors, gradually rising the reaction temperature and vacuum to allow for removal of condensates and compensate for the increasing melt viscosity.[4] PET resins with higher IV (>0.7 dL g^{-1}) are produced through solid state polymerization (SSP). SSP processes essentially involve the heating of polymer particles to 200–240°C for 10–30 h under inert gas flow or vacuum.[5–10] Among its many advantages, SSP also favors the simultaneous removal of acetaldehyde, which can be formed at high reaction temperatures.[11]

To avoid sticking or sintering of prepolymer particles during SSP, cold crystallization (annealing) precedes. Amorphous PET (APET) is heated above its glass transition temperature ($T_g \cong 78$°C) and spontaneous spherulitic crystallization occurs in the solid state.[11–13] In general, crystallization may involve two stages, the primary and secondary crystallization (SC). SC results from crystallites impingement at the end of primary crystallization[14] and may occur since the early stages of crystal growth,[13–16] affecting the physical and mechanical properties of the final product and consequently the posterior molding conditions. For example, melting point (T_m) of secondary crystals increases with increasing heating rate (HR), whereas the T_m of primary crystals decreases under similar conditions. Thus, with the increase of the HR from 2.5 to 80°C min^{-1}, the T_m of the primary PET crystals is lowered by about 20°C, whereas the T_m of the secondary crystals is increased by about 3°C. In addition, the secondary crystals prevent the primary crystals from recrystallizing, whereas SC is known not to comply with the kinetic Avrami equation. Finally, the crystallization rate

Correspondence to: C. D. Papaspyrides (kp@softlab.ece.ntua.gr).

TABLE I
PET Resin Intrinsic Viscosity (IV) Requirement per Application[3]

Application	IV (dL g^{-1})
Textile fibers	0.57–0.65
Bottles	0.72–0.85
Trays	0.85–0.95
Tire cords	0.95–1.05

increases monotonically with increasing temperature when SC dominates, whereas it passes through a maximum during primary crystallization.[14,15]

Obviously, crystallization also takes place during SSP, because particles are heated at temperatures higher than T_g. This crystallinity increase is accompanied by molecular weight build-up, which is found to exert an adverse effect on crystallization at low SSP temperatures (<210°C) as a result of increased entanglements and induced restrictions in segmental mobility.[17–19] Furthermore, the crystallinity of the SSP product (preform) should be kept low, as higher T_m values lead to higher injection molding temperatures and higher acetaldehyde contents in the preforms.[11] For this reason, comonomers, such as isophthalic acid and cyclohexanedimethanol, are used to reduce the crystallizability of the base prepolymer.[4,11]

Existing literature focuses primarily on the crystallinity degree and crystallizability of the final SSP PET product or PET grades produced through long reaction times. The reported crystallinity values (x_c) range from 25 wt % to 67 wt % for number-average molecular weights ($\overline{M_n}$) up to 48,400 g mol^{-1} (IV = 1.15 dL g^{-1}, phenol–tetrachloroethane 3 : 2%, w/w, 25°C) at SSP temperatures ranging from 180 to 245°C and reaction times up to 20 h (Table II). It is interesting also to note that different dynamic x_c trajectories have been reported during the SSP: x_c has been found to remain constant,[20] to increase significantly within the first few hours of reaction before final stabilization[21,22] and even to decrease during the SSP.[23] The distinct x_c behavior has been attributed to the different reaction parameters, such as the used catalysts, the presence of contaminants, the thermal history of the prepolymer, among others.[24]

Part of the SSP PET literature focuses on the effects of initial and increasing polymer crystallinity on the observed reaction rates.[5,17,22] First, the increase of crystallinity leads to higher concentration of end groups in the amorphous phase and thus to an increase of the reaction rates.[6,19] On the other hand, the mobility of the polymer chains is believed to decrease with the degree of crystallinity,[25] which can lead to the simultaneous reduction of removal of by-products from the reacting mass.[26] Duh[22] reviewed the works in the field and highlighted that SSP rates can increase with the degree of crystallinity at 220°C in both pellets and powder, due to the decrease of the inactive end groups concentration in the amorphous phase.

All works cited previously examined the thermal PET properties during or after long SSP times, presenting the final melting behavior of the resin, neglecting however the fact that the most important crystallization phenomena take place rapidly in the early moments of the SSP. For this reason, this article investigates the evolution of crystal morphology and polymer crystallinity during the initial SSP stages (0–2 h) under typical commercial conditions. Short reaction times were selected to minimize the effects of molecular weight build-up on the crystallization process even at low SSP temperatures and to distinguish between primary and secondary crystal formation. SC is of great importance because of the different properties of the final crystals, as mentioned before. Besides, analysis of SC can be relevant for study of crystallization kinetics during the SSP. The Avrami equation has been used very often[17,27] to represent the primary crystallization, although the use of an empirical linear law has also been proposed,[19,28] assuming that the crystallization rate is

TABLE II
PET SSP Literature on Attained Mass Fraction Crystallinity (x_c) and Number-Average Molecular Weights ($\overline{M_n}$)

Reference	SSP conditions	x_c (%)	$\overline{M_n}$ (g mol^{-1})
18[a]	230°C	0.63	19,800
	20 h		
20	215–245°C		
	12 h	0.42[b]	
1[a]	12 h		
	180°C	0.42[b]	21,900
	190°C	0.43[b]	25,800
	200°C	0.44[b]	29,400
	210°C	0.46[b]	32,600
	220°C	0.53[b]	38,200
	230°C	0.57[b]	46,000
22[a]	220°C	0.57[b]	40,600
	20 h	0.59[b]	42,300
		0.62[b]	45,300
		0.67[b]	48,400
23	230°C		
	0 h	0.34[c]	14,400
	4 h	0.31[c]	20,000
	10 h	0.30[c]	22,900
	20 h	0.25[c]	24,600

[a] Estimation was made based on paper figures.
[b] Volume fraction crystallinity (x_v) was converted to mass fraction crystallinity (x_c) through the formula $x_c = \left(\frac{\rho_c \rho_a}{\rho} - \rho_c\right)/(\rho_a - \rho)$, where $\rho = x_v(\rho_c - \rho_c) + \rho_a$ is the polymer density (g cm^{-3}), ρ_c =1.455 g cm^{-3} the density of the crystalline phase, and ρ_a =1.355 g cm^{-3} the density of the amorphous phase.
[c] $\Delta H_0 = 135$ J g^{-1}.[11]

proportional to the weight fraction of crystallizable amorphous material and taking into account the SC. On the other hand, a number of particle models[29,30] assume that crystallinity does not depend on the reaction time and is a function of temperature only.

EXPERIMENTAL

Initial PET material

Amorphous cylindrical PET pellets (prepolymer), with average diameter of 1 mm and average height of 2 mm, were kindly supplied by BRASKEM (Camaçari, Brazil). PET pellets were produced through transesterification and contained very low carboxylic contents. Small amounts of isophthalic acid oligomer (1.99–2.50 ± 0.02 mol %) were incorporated into the resin to reduce the final crystallinity of the PET product. The IV of the prepolymer was equal to 0.620 ± 0.08 dL g^{-1} in 1,1,1,3,3,3-hexafluoroisopropanol (HFIP). Before any SSP run, the samples were dried overnight (60°C, in vacuum) and 2 g of prepolymer were used for SSP reactions.

Solid state polymerization runs

A bench scale reactor, assembled by INVISTA Inc., was used to solid state polymerize PET at various times and temperatures under flowing nitrogen (Table III). The cylindrical, stainless steel reactor was equipped with a gas inlet below the sample chamber, to permit preheated purge gas (nitrogen, N_2 purity 99.999%) to pass through the polymer bed during reaction. The purge gas was used to distribute heat evenly throughout the sample chamber and to remove volatile reaction products. The nitrogen, controlled at a constant predetermined flow rate through a calibrated flowmeter, was preheated while passing through a coil of 1/8 in. stainless steel tubing. Thermocouples at two individual locations within the reaction chamber were used to monitor polymer temperature during SSP. A fluidized sand bath (Techne Corp., Minneapolis, USA) was used to heat the reactor and the purge gas.

The reactor was first filled with dried prepolymer, closed, and examined for leaks through a pressure test. The temperature of the sand bath was raised to the SSP temperature (T_{SSP}), and the reactor was immersed in the fluidized bath. The initial reaction condition ($t_0 = 0$ min) was assumed to be the moment when the reactor reached the T_{SSP}. This way, the effect of the heating time could be neglected in this study and the properties of the grades at zero time corresponded to the resin properties at t_0. After completion of the reaction run, the reactor was cooled ($T < 80$°C), the product was removed from the reactor vessel, placed in a plastic container, sealed, and stored in a desiccator.

TABLE III
PET SSP Experimental Conditions

T_{SSP} (°C)	N_2 flow rate (mL min^{-1})	t (min)
184	285	0, 20, 40, 60, 120
220	285	0, 10, 20, 40, 60, 120
230	285	0, 10, 20, 40, 60, 120

Characterization

Intrinsic viscosity measurements

Samples were pulverized, using the mill PULVERISETTE 14 (FRITSCH Corp., Idar-Oberstein, Germany). IV was measured in HFIP at a concentration of 0.50 g dL^{-1} in a Canon–Fenske–Ostwald capillary viscometer at 30 ± 0.1°C. The IV value was obtained with the single point technique [eq. (1)], as proposed by Billmeyer[31]:

$$\mathrm{IV} = \frac{1}{4}\frac{\eta_{sp}}{C} + \frac{3}{4}\frac{\ln \eta_{rel}}{C} \quad (1)$$

where C is the polymer concentration (g dL^{-1}), η_{sp} is the solution specific viscosity, and η_{rel} is the solution relative viscosity. Measurements were performed in duplicates. The IV values were converted to molecular weight through the Mark–Houwink–Sakurada equations[32]:

$$\mathrm{IV} = 4.86 \times 10^{-4}\overline{M_n}^{0.72} \qquad (\overline{M_n} > 16{,}000 \text{ g mol}^{-1}) \quad (2)$$

$$\mathrm{IV} = 6.93 \times 10^{-3}\overline{M_n}^{0.48} \qquad (\overline{M_n} < 16{,}000 \text{ g mol}^{-1}) \quad (3)$$

where IV is given in dL g^{-1} and $\overline{M_n}$ is the number-average molecular weight of the polymer sample, given in g mol^{-1}.

Thermal properties

Differential scanning calorimetry (DSC) measurements were performed in a Perkin–Elmer instrument (DSC 6) with HR of 10°C min^{-1} under nitrogen flow (20 mL min^{-1}). All measurements were performed in duplicates. The melting behavior of APET and bottle-grade PET (BPET) obtained after the industrial SSP were used as references. The degree of crystallinity was computed as described in eqs. (4) and (5). Equation (5) is used when a cold crystallization exotherm is detected in the DSC scans, as in the case of APET (Fig. 1):

$$x_c = 100 \times \frac{\Delta H_f}{\Delta H_0} \quad (4)$$

$$x_c = 100 \times \frac{(\Delta H_f - \Delta H_c)}{\Delta H_0} \quad (5)$$

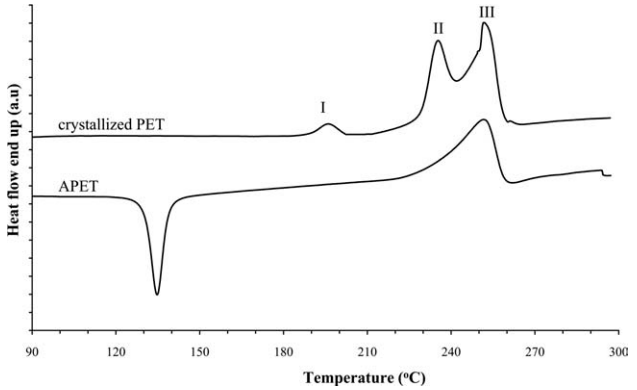

Figure 1 Typical DSC scans of amorphous (APET) and crystallized PET presenting multiple melting behavior (Endotherms I–III).

where ΔH_c is the heat of crystallization observed during the scan (J g^{-1}), ΔH_f is the heat of fusion calculated from the melting peak (J g^{-1}), and ΔH_0 is the heat of fusion of 100% crystalline polymer (J g^{-1}). For PET, ΔH_0 is considered equal to 135 J g^{-1}.[11]

Wide-angle X-ray diffraction (WAXD)

Samples were pulverized, using the mill PULVERISETTE 14 (FRITSCH Corp., Idar-Oberstein, Germany). WAXD spectra were collected from a Rigaku Mini-Flex RIX 3100 Diffractometer (Rigaku, Tokyo, Japan), equipped with a Cu Kα radiation ($\lambda = 0.154$ nm), operating at 30 kV, 15 mA.

RESULTS AND DISCUSSION

Theoretical

Multiple melting behavior (Endotherms I–III, as shown in Fig. 1) is commonly found in crystallized PET; depending on crystallization conditions, the number and the temperatures of endotherms vary. In general, this multiple melting behavior is explained on the basis of two main approaches, which obey the crystallization model of dominant-parent lamellar crystals and subsidiary branches.[33–35] According to the first approach, the effect of thermal scanning during DSC is significant and may lead to high melting species: the first endotherm (I) is associated to SC or thinner/imperfect lamellae,[36] the second peak (II) is related to the isothermally grown crystals or dominant lamellae, and the third one (III) is the result of the solid state reorganization that takes place during the linear heating of the DSC scan.[14,16,36–40] According to the second approach, the DSC heating effect is less significant. The low temperature peaks (I and II) are attributed to SC or incomplete structures, which already exist in the material before DSC scanning. The third endotherm (III) is assigned to relatively complete structures or parent-dominant crystals, which under DSC linear heating would also undergo some reorganization in terms of lamellar thickening.[33,35,38]

The multiple melting behavior of PET samples obtained at the end of the SSP process was analyzed by Kim et al.,[21] who found two endotherms for the SSP products after 12 h in the temperature range of 180–230°C. The second endotherm was attributed to the solid state reorganization that takes place during the DSC scan; however, this effect could not be proved and the correlation between the crystallization phenomena and the SSP time was not thoroughly analyzed.

Melting behavior of SSP grades

As shown in Figure 2, the IV lift ($\Delta IV = IV_t - IV_{A\text{-}PET}$) at the end of 2 h of SSP varied from 0.018 to 0.125 dL g^{-1}, depending on the reaction temperature. From a practical point of view, the IV did not increase significantly at 184°C and the number-average molecular weight ($\overline{M_n}$) remained constant and equal to 12,300 g mol^{-1}. At higher temperatures (220°C and 230°C), a more important growth of IV was observed, leading to $\overline{M_n}$ values of 26,200 and 26,600 g mol^{-1}.

The most important thermal properties of SSP samples are presented in Table IV, which includes the APET and the BPET. Multiple melting behavior was observed (Peaks I–III) in the SSP products. First, the effect of DSC linear heating on the grade morphology and crystallinity was analyzed by applying different DSC HRs, as recommended in the literature.[35,41] As it can be seen in Figure 3, the melting points related to Peak II shifted more slightly (nearly 5°C) as a function of HR than with the isothermal SSP temperature as observed in Table IV. Therefore, although the effect of HR is not very significant, the

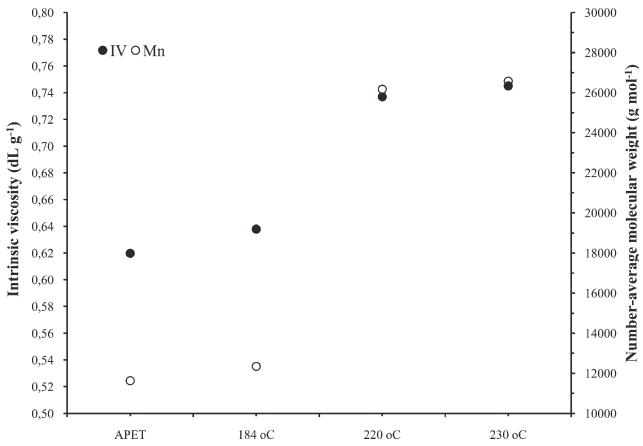

Figure 2 Intrinsic viscosity (IV) and number-average molecular weight ($\overline{M_n}$) of PET SSP grades after 2 h.

TABLE IV
Thermal Properties of SSP Grades Determined Through DSC Under HR of 10°C min^{-1}

		T_c (°C)	ΔH_c (J g^{-1})	T_{II} (°C)	T_{III} (°C)	$\Delta H_{f(II+III)}$ (J g^{-1})
APET		133.2 ± 6.8	26.1 ± 8.3		253.0 ± 2.6	53.3 ± 8.5
BPET				244.3 ± 2.6	250.6 ± 2.0	77.6 ± 27.6
t_{SSP} (min)	Peak I		Peaks II and III			
	T_I (°C)	ΔH_I (J g^{-1})	T_{II} (°C)	T_{III} (°C)	$\Delta H_{f(II+III)}$ (J g^{-1})	$\Delta H_{f(I,II+III)}$ (J g^{-1})
T_{SSP} = 184°C						
0	189.0 ± 0.9	1.6 ± 0.3	–	252.2 ± 0.7	38.0 ± 7.9	39.6 ± 8.2
20	193.4 ± 0.3	2.8 ± 0.2	–	251.7 ± 2.1	41.4 ± 5.7	44.3 ± 6.0
40	196.2 ± 0.2	3.3 ± 1.4	–	253.6 ± 0.1	46.0 ± 4.4	49.3 ± 5.8
60	198.0 ± 0.9	2.5 ± 1.6	–	253.7 ± 1.8	46.1 ± 14.2	48.6 ± 12.7
120	203.4 ± 0.7	1.9 ± 0.4	–	252.6 ± 3.0	44.1 ± 9.5	46.1 ± 9.1
T_{SSP} = 220°C						
0			229.1 ± 1.6	251.6 ± 2.5	47.8 ± 20.2	47.8 ± 20.2
10			231.4 ± 1.2	250.9 ± 1.4	43.1 ± 4.3	43.1 ± 4.3
20			232.0 ± 2.0	251.3 ± 3.0	46.7 ± 1.1	46.7 ± 1.1
40			235.3 ± 0.4	252.9 ± 2.9	50.0 ± 10.5	49.9 ± 10.5
60			237.6 ± 1.4	252.0 ± 3.6	55.8 ± 8.0	55.8 ± 8.0
120			239.0 ± 1.4	250.4 ± 0.0	50.8 ± 14.1	50.8 ± 14.1
T_{SSP} = 230°C						
0			238.6 ± 0.1	251.5 ± 1.4	47.5 ± 16.2	47.5 ± 16.2
10			243.4 ± 1.6	253.3 ± 1.4	56.4 ± 6.0	56.4 ± 6.0
20			243.6 ± 0.7	254.1 ± 1.4	57.9 ± 4.5	57.9 ± 4.5
40			246.8 ± 1.6	253.4 ± 0.0	54.4 ± 12.3	54.4 ± 12.3
60			248.6 ± 0.7		55.5 ± 4. 5	55.5 ± 4.5
120			252.4 ± 2.0		52.7 ± 20.0	52.7 ± 20.0

endotherms observed in the grades are somewhat influenced by heating during DSC scan, indicating first that samples suffer some sort of reorganization and/or reorientation during the DSC analysis, and second that secondary crystals are formed, because T_m is slightly increased with HR, as already mentioned in Introduction.

The effect of the DSC scan on the crystallinity of SSP samples at the studied HR (10°C min^{-1}) was also analyzed by comparing the DSC values with those derived from WAXD analysis (Fig. 4). The degree of crystallinity (x_c) obtained through DSC analysis was found to be systematically higher than the values obtained by WAXD, but followed in principal the same trends considering also the relatively higher DSC errors. Discrepancies between crystallinity values estimated from these techniques have been reported previously[42] and depend on the deconvolution method used to interpret the WAXD diffractograms. Besides, the degree of crystallinity obtained through DSC analyses depends on selection of the baseline and on integration of thermograms between limits which cannot be defined unambiguously. This problem can be magnified in the case of samples with

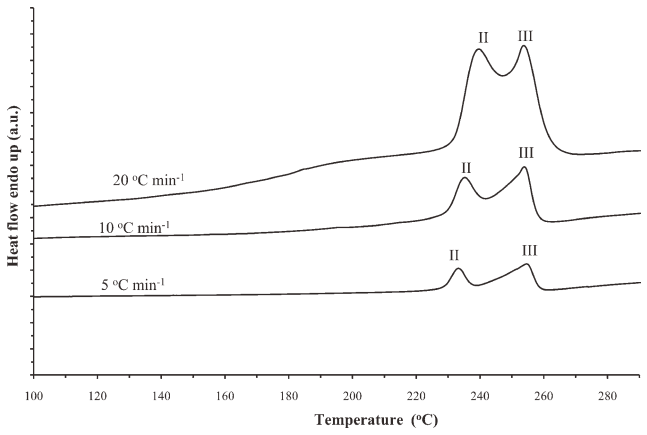

Figure 3 DSC heating rate effect on PET melting behavior (T_{SSP} = 220°C; 40 min).

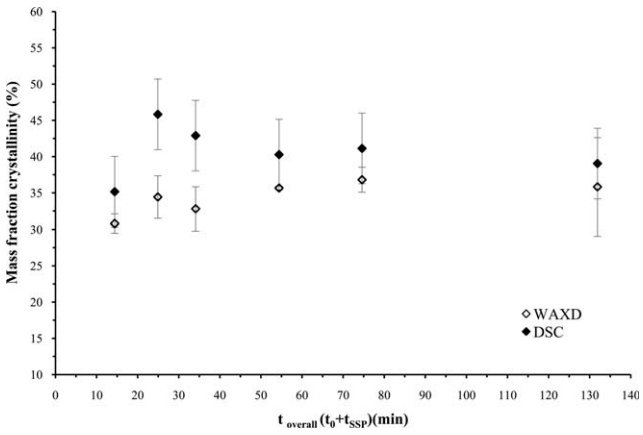

Figure 4 DSC and WAXD measured mass fraction crystallinity of PET grades at T_{SSP} = 230°C (HR = 10°C min^{-1}).

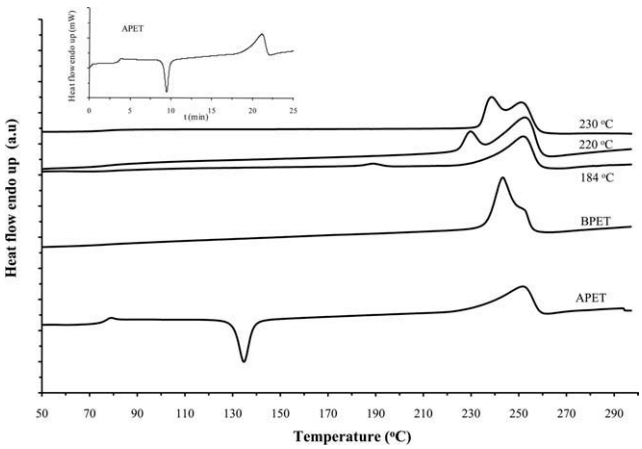

Figure 5 DSC scans (HR = 10°C min^{-1}) of amorphous PET (APET), bottle-grade PET (BPET), and PET SSP grades at the end of SSP heating period (t_0; T_{SSP} = 184, 220, and 230°C).

low crystallinity because the heat flow contribution from heat capacity changes ($\int_{T_c}^{T_m} C_p(T)dT$) can be subject to significant uncertainty; for this reason, in this work the total heat flow provided by the DSC equipment was used for calculations.[11]

Crystal morphology of SSP samples

DSC data are quoted in Figure 5 for APET, BPET, and SSP samples collected at the end of the SSP heating period (t_0). In the case of APET, a prominent T_g (75.1 ± 1.8°C) appeared, followed by cold crystallization with a well-defined exothermic peak (T_c) at 133.2 ± 6.8°C and enthalpy value (ΔH_c) 26.1 ± 8.3 J g^{-1}. At the selected DSC HR of 10°C min^{-1}, cold crystallization was completed after 10 min, which is anticipated to decrease as HR increases, due to the shorter time period and faster nuclei activation. A broad endotherm followed at 253.0 ± 2.6°C with melting enthalpy (ΔH_f) of 53.3 ± 8.5 J g^{-1}, lying in the referred limits of 35–65 J g^{-1} for all types of PET.[11] Based on ΔH_f and ΔH_c, the initial crystallinity of prepolymer samples was equal to x_c of 19 ± 6%, which may be attributed either to the relatively low DSC accuracy or more probably to quenching and storage conditions of the APET, prepared by melt polymerization.[11,41] BPET exhibited a shoulder endotherm peak (II: 244.3 ± 2.6°C and III: 250.6 ± 2.0°C) with a total degree of crystallinity of 58 ± 18%.

The DSC scans of SSP products at t_0 did not show any exothermic peak, indicating that cold crystallization occurred very rapidly during the SSP heating time, which was always higher than 11 min. This prepolymer crystallization was in fact favored by the HR in the reactor during the first SSP stage (17 ± 5°C min^{-1}) which was higher than the HR at DSC scans, and the SSP temperatures (184–230°C), being higher than the observed cold crystallization exotherm of APET.

All remaining SSP grades were characterized by multiple melting peaks, the values and morphology of which varied as a function of SSP temperature and time (Table IV). More specifically, SSP temperature emerged as a critical parameter for PET melting behavior, as shown in Figure 6. At the low SSP temperature, 184°C, a weak peak (I) appeared at 10°C higher than the SSP temperature, varying between 189.0 and 203.4°C and increasing with SSP time [Fig. 6(a)], but with low enthalpy values (1.6–3.3 J g^{-1}). Peak I can be attributed to SC in the early stages of growth during nonisothermal and isothermal solid-phase reaction. Then, a prominent broad endotherm (III), similar to APET, was found at 251.7–253.7°C [Fig. 6(b)] and can be related to primary PET crystals formed during the nonisothermal SSP heating.

At the higher SSP temperatures, Peak I weakened significantly and disappeared; meanwhile, binodial peaks were observed in the range of 229.1–254.1°C. Peak II can also be attributed to SC and considered equivalent to Peak I at 184°C, which moved to higher melting temperatures, closer to the main BPET melting point (244.3°C), due to larger molecular mobility and higher SC rate. The broad Peak III,

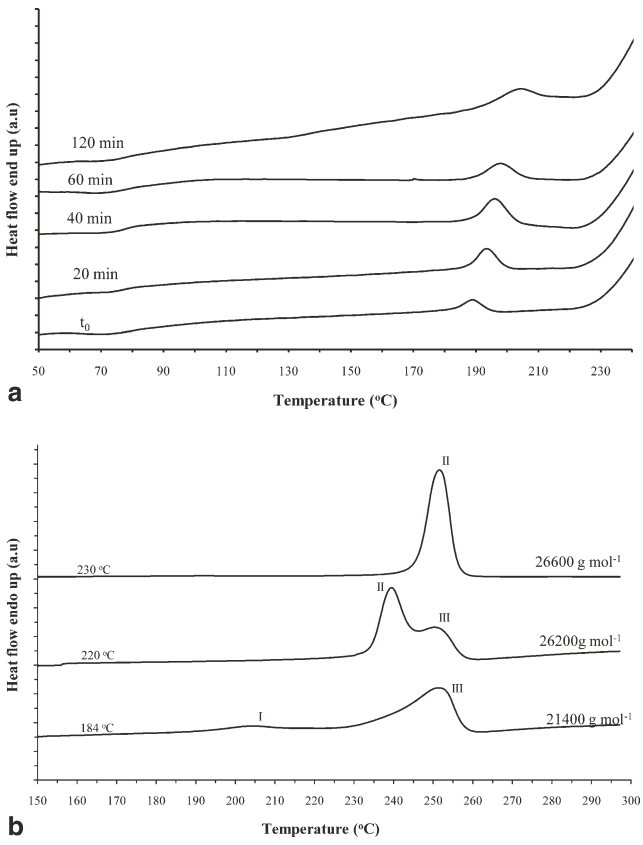

Figure 6 DSC scans (HR = 10°C min^{-1}) of PET SSP grades during isothermal reaction (a) at 184°C and (b) after 120 min at the three SSP temperatures.

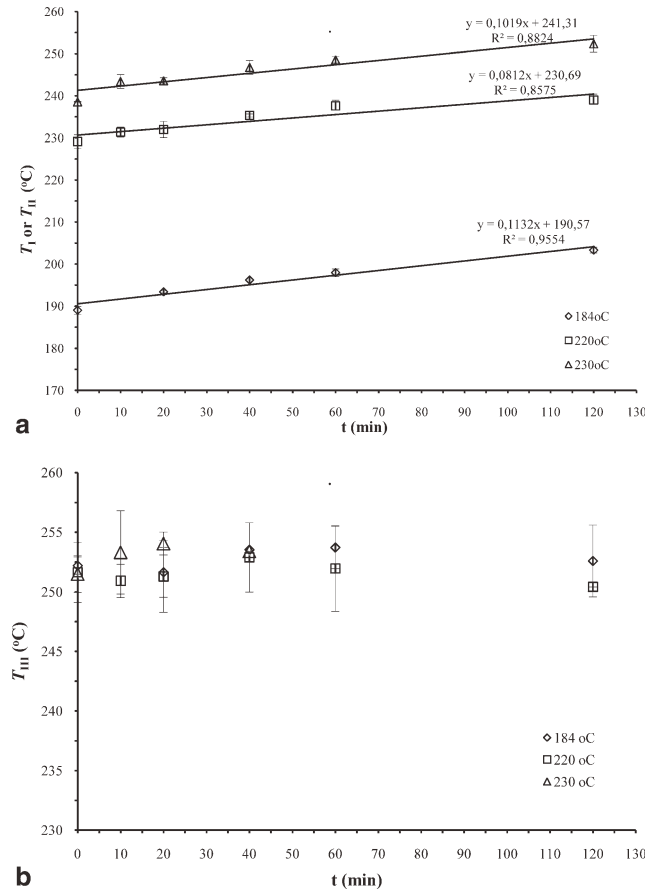

Figure 7 Change of melting peaks as a function of SSP reaction time (a) I and II endotherms (T_I or T_{II}) and (b) III endotherm (T_{III}).

corresponding to parent crystals, formed mainly during the nonisothermal SSP heating period, decreased in height and broadened in the benefit of Peak II. At 230°C, Peak III almost disappeared, showing that secondary crystals were formed early in high quantities, being thus the dominant structure in the SSP product. As a result, the higher the SSP temperature, the faster the SC due to enhanced segmental mobility, leading to thickening and larger amounts of pertinent crystals and changing the behavior from two or three to one melting endotherm.

The observed melting behavior of PET samples as a function of SSP temperature can be correlated to the attained molecular weights: the higher the MW of PET, the greater the rejection of chain sections in interlamellar regions. This rejection leads to higher secondary nucleation sites and supports the SC model, which involves the formation of an intermediate crystalline structure in the middle of two parent crystals.[33]

The SC model can also be verified by studying the effect of SSP time on crystals morphology. Peaks (T_I or T_{II}), corresponding to SC, consistently increased with the reaction time [Fig. 7(a)], as a result of the solid-phase reorganization.[15] On the contrary, the melting points (T_{III}) of the primary-parent crystals were constant with time [Fig. 7(b)]. This indicates that the secondary crystals were not included in the primary ones. If SC was a simple continuation of the primary crystallization, leading to additional crystallization or modification of crystallites, SC would surely modify the melting behavior of the primary crystals.[15] The latter indicates a possible crystallization model involving the formation of secondary crystals within interlamellar regions or in the borders of primary crystals, resembling to amorphous bodies.[13,15]

Furthermore, T_I or T_{II} were also found to increase linearly as a function of SSP time, allowing for estimation of the melting point of the final SSP product (T_m) under the selected temperature conditions. An empirical equation was built, expressing T_m as a function of SSP temperature and time [eq. (6)]. In particular, in eq. (6), the average value of the linear regression slopes of T_I or T_{II} versus t data was used, whereas the relevant intercept was found to be an exponential function of SSP temperature, allowing for excellent fitting of available data (Fig. 8). Equation 6 can be used to control the melting point of the SSP product at plant site, in the benefit of subsequent processing stages:

$$T_m = 0.10 \times t + 2544.27 \times \exp\left(\frac{-9845.44}{RT}\right) \quad (6)$$

where T_m is the melting point due to SC (°C), T the SSP temperature (K), t the SSP time (min), and R the gas universal constant (J mol^{-1} K^{-1}).

Finally, examining the effect of the isophthalic comonomer on the crystals morphology, it has been well-established that the crystallization of PET homopolymer occurs by formation of spherulitic crystallites [11–13,43]. In this case, the increase of the

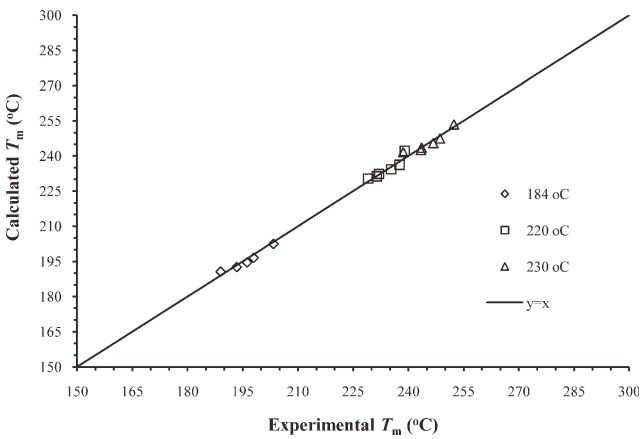

Figure 8 Fitting of eq. (6) to experimental data.

spherulite radius should increase linearly over time at a fixed temperature, as described by Mandelkern.[44] The linear behavior observed here indicates that the crystallites growth is surface-controlled and not diffusion-controlled, as described in the literature for PET homopolymer, and reveals that the PETI heteropolymer investigated in this work presents a thermal behavior that is similar to the thermal behavior of PET homopolymers,[40,45] probably because of the low comonomer content. PETI presents some conformational deviations from the linear structure of PET homopolymer chains, which leads to deacceleration of the crystallization kinetics.[46] Despite that, the triple melting behavior and molecular weight effects observed here for PETI are analogous to the effects reported for PET resins, probably due to the ranges of comonomer composition considered. Nobuo et al.[47] have claimed that none of isophthalate composition exists in crystalline region when PETI contains less than 10% isophthalate. Therefore, the N-isopropylacrylamide comonomer units would be likely contained in the amorphous regions of copolymer studied in this work, contributing no significantly to morphological changes at this level of concentration.

Crystallinity of SSP samples

After 2 h of SSP, the degree of crystallinity ranged from 34.1 to 39.0 wt % (Fig. 9 and Table II). x_c values were found to increase with the SSP temperature and final IV but were apparently lower than the degree of crystallinity obtained for BPET polymerized at the industrial BRASKEM site, certainly due to the different operation conditions.

According to Figure 9, the total degree of crystallinity increased up to 29.3–35.2% during the SSP heating time (t_0), a value that corresponds both to primary and SC. Further increase occurred during isothermal solid state reactions at 184 and 220°C for the period of 40–60 min, whereas for longer reaction times, x_c remained essentially constant. More specifically, at 184°C, the crystallinity trend coincided with the variation of x_c related to Peak I, which was assigned to the secondary crystals. It seems that during the early stages of SC, the formation of secondary crystals population imparted higher crystallinity degree maintaining also the presence of parent crystals.

At a first glance, Figure 9 could suggest that SC has produced a maximum degree of crystallinity, and thereafter this property tends to decrease potentially due to a physical stability loss (disturbing). However, these maximum crystallinity values could be explained in terms of the DSC uncertainties, as reported by Bashir et al.[11] In fact, when comparing the crystallinity data obtained at 230°C and shown in Figure 9 to the data presented in Figure 4, it can be noted that points of DSC maximum crystallinity could not be detected by WAXD. Besides, the error bars are relatively large (>5%) and indicate that the points of maximum can constitute a numerical artifact, due to unavoidable measurement uncertainties. It is also important to emphasize that SSP products present some heterogeneity due to the residence time distributions, which can also contribute with some scattering of data values. On the other hand, melting points can be determined with high precision as clearly demonstrated in Figure 7(a), lending confidence to the SSP morphology findings discussed earlier.

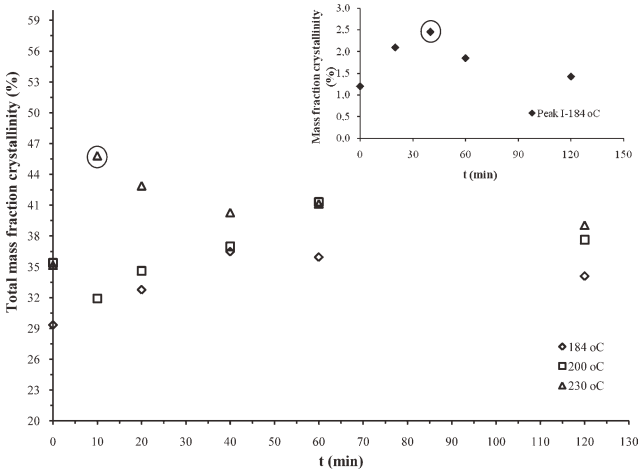

Figure 9 Degree of crystallinity of SSP PET grades as a function of SSP time.

Despite DSC uncertainty, a linear function could be built to correlate the final reached x_c values after 2 h of reaction and the reaction temperature [eq. (7); $R^2 = 0.9946$), as also suggested by Mallon and Ray.[19] This supports the assumption of constant crystallinity in SSP particle models, because crystallinity was proved to change during an initial short period of SSP time (up to 60 min) and then stabilized, being only a function of SSP temperature.

$$x_c = 0.3543 + 0.001(T - 470) \quad (7)$$

where T is the SSP temperature (K) and x_c the mass fraction crystallinity.

CONCLUSIONS

During SSP processes PET crystallizes rapidly. The annealing process was studied here under real industrial SSP conditions and correlated to reaction temperature, reaction time and increase of molecular weight. It was found that SC occurred since the early stages of crystal growth. The DSC results suggest that the size and shape of secondary crystals

strongly depended on SSP temperature: at low temperature, SC rates were low and low melting crystals were formed. At higher SSP temperatures, the enhanced segmental mobility and higher lateral spreading rate resulted in higher melting and larger secondary crystals. Similarly, SSP time exerted a positive effect on solid-phase perfection of secondary crystals, leading at each temperature to melting points close to T_m of BPET. An empirical equation for melting point assessment as a function of SSP time and temperature was successfully constructed and applied, whereas final crystallinity degree was found linearly proportional to reaction temperature.

References

1. The compelling facts about plastics. Plastics Europe; Association of Plastics Manufacturers Publication, January 2008.
2. East, A. In Encyclopedia of Polymer Science and Technology; John Wiley & Sons: NJ, 2002.
3. Duh, B. J Appl Polym Sci 2001, 81, 1748.
4. Wadekar, S.; Agarwal, U.; Boon, W.; Nadkarni, V. In Solid State Polymerization; Papaspyrides, C.; Vouyiouka, S., Eds.; John Wiley & Sons: NJ, 2009, Chapter 8.
5. Papaspyrides, C.; Vouyiouka, S. Solid State Polymerization; John Wiley & Sons: NJ, 2009.
6. Ravindranath, K.; Mashelkar, R. J Appl Polym Sci 1990, 39, 1325.
7. Ma, Y.; Agarwal, U.; Sikkema, D.; Lemstra, P. Polymer 2003, 44, 4085.
8. Duh, B. Polymer 2002, 43, 3147.
9. Duh, B. Polymer 2002, 43, 1748.
10. Zhi-Lian, T.; Qiu, G.; Huang, N.; Claudio, S. J Appl Polym Sci 1995, 57, 473.
11. Bashir, Z.; AL-Aloush, I.; AL-Raqibah, I.; Ibrahim, M. J Polym Eng Sci 2000, 40, 2442.
12. Roberts, R. Polymer 1969, 10, 117.
13. Wellen, R.; Rabello, M. J Mater Sci 2005, 40, 6099.
14. Zheng, K.; Yao, X.; Chen, L.; Tian, X. J Macromol Sci B Phys 2009, 48, 318.
15. Yagparov, M. J Therm Anal 1986, 31, 1073.
16. Tian, X.; Ruan, C.; Cui, P.; Liu, W.; Zheng, J.; Zhang, X.; Yao, X.; Zheng, K.; Li, Y. J Macromol Sci B Phys 2006, 45, 835.
17. Medellin-Rodriguez, F.; Lopez-Guillen, R.; Waldo-Mendoza, M. J Appl Polym Sci 2000, 75, 78.
18. James, N.; Ramesh, C.; Sivaram, S. Macromol Chem Phys 2001, 202, 1200.
19. Mallon, F.; Ray, W. J Appl Polym Sci 1998, 69, 1233.
20. Wu, D.; Chen, F.; Li, R.; Shi, Y. Macromolecules 1997, 30, 6737.
21. Kim, T.; Lofgren, A.; Jabarin, S. J Appl Polym Sci 2003, 89, 197.
22. Duh, B. J Appl Polym Sci 2006, 102, 623.
23. Yu, H.; Han, K.; Yu, M. J Appl Polym Sci 2004, 94, 971.
24. Jabarin, S. J Appl Polym Sci 1987, 34, 85.
25. Fakirov, S.; Avramova, N. Acta Polym 1982, 33, 271.
26. Li, L.; Huang, N.; Liu, Z.; Tang, Z.; Yung, W. Polym Adv Technol 2000, 11, 242.
27. Kang, C. J Appl Polym Sci 1998, 68, 837.
28. Wang, X.; Deng, D. J Appl Polym Sci 2002, 83, 3133.
29. Goodner, M.; Gross, S.; DeSimone, J.; Roberts, G.; Kiserow, D. J Appl Polym Sci 2001, 79, 928.
30. Kim, T.; Jabarin, S. J Appl Polym Sci 2003, 89, 213.
31. Billmeyer, F. J Polym Sci 1949, 4, 83.
32. Ohoya, S.; Hasegawa, T.; Tsubakiyama, K.; Matsuo, T. Polym J 2001, 33, 113.
33. Medellin-Rodriguez, F.; Phillips, P.; Lin, J. Campos J Polym Sci B Polym Phys 1998, 35, 1757.
34. Bell, J.; Murayama, T. J Polym Sci A-2 1969, 7, 1059.
35. Medellin-Rodriguez, F.; Phillips, P. Macromolecules 1996, 29, 7491.
36. Zhou, Ch.; Clough, S. Polym Eng Sci 1988, 28, 65.
37. Holdsworth, P.; Turner-Jones, A. Polymer 1971, 12, 195.
38. Raheil, I. Polym Int 1994, 35, 189.
39. Groeninckx, G.; Reynaers, H.; Berghmans, H.; Smets, G. J Polym Sci Polym Phys Ed 1980, 18, 1311.
40. Groeninckx, G.; Reynaers, H. J Polym Sci Polym Phys Ed 1980, 18, 1325.
41. Schawe, J. Thermochim Acta 2007, 145.
42. Murthy, N.; Khanna, Y.; Signorelli, A. Polym Eng Sci 1994, 3, 1254.
43. Lu, W.; Debelak, K.; Witt, A.; Yang, C.; Collins, W.; Lott, C. J Polym Sci B Polym Phys 2002, 40, 245.
44. Mandelkern, L. CrystalIization of Polymers—Kinetics and Mechanisms; Cambridge University Press: Cambridge, 2004.
45. Avila-Orta, C.; Medellin-Rodriguez, F.; Wang, Z.-G.; Navarro-Rodriguez, D.; Hsiao, B.; Yeh, F. Polymer 2003, 44, 1527.
46. Holland, B.; Hay, J Polymer 2002, 43, 1797.
47. Nobuo, U.; Yasuhiko, N.; Rei, Y. Chem High Polym (Jpn) 1964, 21, 729.